IOP Publishing Journal of Physics D: Applied Physics
J. Phys. D: Appl. Phys. **48** (2015) 205402 (14pp) doi:10.1088/0022-3727/48/20/205402

# Design of a triangular platform piezoresistive affinity microcantilever sensor for biochemical sensing applications

**Ribu Mathew and A Ravi Sankar**

MEMS Laboratory, School of Electronics Engineering (SENSE), VIT Chennai, Chennai 600 127, India

E-mail: ribumathew88@gmail.com and a.ravishan@gmail.com

Received 22 December 2014, revised 6 March 2015
Accepted for publication 16 March 2015
Published 21 April 2015


**Abstract**

Microcantilever platforms with integrated piezoresistors have found versatile applications in the field of clinical analysis and diagnostics. Even though treatise encompasses numerous design details of the cantilever based biochemical sensors, a majority of them focus on the generic slender rectangular cantilever platform mainly due to its evolution from the atomic force microscope (AFM). The reported designs revolve around the aspects of dimensional optimization and variations with respect to the combination of materials for the composite structure. In this paper, a triangular cantilever platform is shown to have better performance metrics than the reported generic slender rectangular and the square cantilever platforms with integrated piezoresistors for biochemical sensing applications. The selection and optimization of the triangular cantilever platform is carried out in two stages. In the first stage, the preliminary selection of the cantilever shape is performed based on the initial design obtained by analytical formulae and numerical simulations. The second stage includes the geometrical optimization of the triangular cantilever platform and the integrated piezoresistor. The triangular cantilever platform shows a better performance in terms of the figure of merit (FoM), $\psi = (\Delta R/R)f_0^2$ and the measurement bandwidth. The simulation results show that the magnitude of $\psi$ of the triangular platform is 77.21% and 65.64% higher than that of the slender rectangular and the square cantilever platforms respectively. Moreover, the triangular platform exhibits a measurement bandwidth that is 70.91% and 2.04 times higher than that of the slender rectangular and square cantilever structures respectively. For a better understanding of the 2D nature of the stress generated on the cantilever platform due to the surface stress, its spatial profile has been extracted and depicted graphically. Finally, a set of design rules are provided for optimizing the triangular cantilever platform and piezoresistor dimensions in terms of the electrical sensitivity and the mechanical stability for biochemical sensing applications.

Keywords: piezoresistive microcantilever, biochemical sensor, surface stress, triangular cantilever

(Some figures may appear in colour only in the online journal)

## 1. Introduction

In micro total analysis system ($\mu$-TAS) and lab-on-a-chip (LOC) applications, microcantilevers are extensively used as mechanical sensing platforms mainly due to the advantages of parallel sensing and batch fabrication. With integration of microelectronics on the same chip they yield an efficient and cost effective point-of-care testing (POCT) system. For specific detection of target species in a given test sample, the microcantilever is coated with receptors either on the top or bottom surface having affinity towards the target species. The detection of the target species is accomplished by either

 © 2015 IOP Publishing Ltd Printed in the UK

sensing the change in the resonant frequency of the structure due to the added mass of the target (dynamic mode) or by measuring the differential stress generated on the cantilever (static mode). Typical examples of the dynamic mode of sensing using a microcantilever platform include detection of airborne nanoparticles [1], DNA [2], volatile organic compounds (VOCs) [3], etc. However, the dynamic mode of sensing suffers from serious limitations due to the dependence of the Q-factor and resonant frequency on the viscosity of the medium of operation [4]. In the static mode of sensing, the target-receptor binding on the cantilever surface generates a mechanical loading on the cantilever, because of which it deflects either upwards or downwards depending on the nature of the stress developed. The differential stress or the deflection of the microcantilever gives the type and the measure of specific target molecule in the test sample. Literature comprises of numerous examples elaborating different detection schemes and quantification methods for the surface stress [5–10]. However, the most widely used methods for measurement of the surface stress induced deflection of the cantilever can be broadly classified as either optical or electrical readout methods.

The optical readout method consists of a light source and a position detection system (PDS) for measuring the deflection of the microcantilever. Optical readout suffers from serious limitations due to the bulkiness of the setup, difficulty in realignment and recalibration (the former in the case of measurements with samples with different refractive index and the latter for repeatability in sensing), and ineffectiveness in opaque samples. As an alternative method, integrated piezoresistive readout, gives a feasible solution by directly transducing the generated surface stress due to the target-receptor binding into an equivalent electrical signal. Piezoresistive readout offers the advantages of real time and label free detection, simple signal conditioning circuitry, large dynamic range, integration with the CMOS fabrication process and medium independence compared to optical and other electrical readout methods like piezoelectric, capacitive etc. Typical applications of piezoresistive microcantilever sensors include DNA sequencing [11], detection of explosives [12], detection of viruses [13], detection of cancer tissues [14], as biosensors [15], as immunosensors [16], as gas density sensors [17] etc.

Even though piezoresistive readout has an edge over other readout methods, the minimum detectable signal i.e. the resolution of the piezoresistive readout is one order less than that of the optical readout method mainly due to the noise constraints. There are mainly two sources of noise in a piezoresistive sensor system: (i) internal noise such as the electrical noise generated in the piezoresistor, mainly the Johnson and the Hooge ($1/f$) noise [18], and (ii) external noise such as mechanical vibration from the environment. The resolution and signal to noise ratio (SNR) of the piezoresistive microcantilever sensors can be made comparable with optical readout by careful design and optimization with respect to the above mentioned noise sources. There are several guidelines for optimizing the electrical noise in the piezoresistor by taking into account the dimensional, doping and process parameters of the piezoresistor design [19–21]. At the measurement level, the symmetric Wheatstone bridge (WSB) with one sensing and one reference cantilever has proven to be effective in nullifying the effects of thermal drifting and background noise [22]. Apart from the aforementioned noise sources, another source of noise is thermo-mechanical noise. The premise results in physical oscillations of the cantilever due to the internal thermal energy. Thermomechanical noise is a function of the cantilever stiffness, resonant frequency, and quality factor [18].

**Table 1.** Design specifications of the proposed piezoresistive microcantilever biochemical sensor.

| Parameter | Value |
|---|---|
| Measurand: Surface stress, $\sigma_s$ ($\mathrm{N\,m^{-1}}$) | 0–100 E-3 |
| Electrical sensitivity, $(\Delta R/R)/\sigma_s$ ($\mathrm{m\,N^{-1}}$) | > 1 E-3 |
| Resonant frequency, $f_0$ (Hz) | > 25 E3 |
| Spring constant, $k_s$ ($\mathrm{N\,m^{-1}}$) | > 100 E-3 |

In this paper, we present a triangular-shaped microcantilever platform with an integrated piezoresistor for biochemical sensing applications. Single crystalline silicon (SCS) with a high doping concentration ($5E19\,\mathrm{cm^{-3}}$) is considered as the piezoresistive element due to its higher piezoresistive coefficients, lower temperature coefficient of sensitivity and reduced noise effects [23] compared to polysilicon [24]. Generally, due to its opposite and comparable magnitude of piezoresistive coefficients a $p$-type silicon piezoresistor is most suited for WSB detection [25]. In the present work, the focus is on designing a mechanical platform which has a high stability against external noises with a higher bandwidth of measurement compared to the conventional rectangular mechanical platforms used for biochemical sensing applications. The design is optimized in terms of maximizing the value of $(\Delta R/R)f_0^2$ (denoted as $\psi$ in the rest of the manuscript), where $R$ is the nominal resistance, $\Delta R$ is the change in resistance and $f_0$ is the resonant frequency. Maximizing $\psi$ ensures maximum electrical sensitivity ($\Delta R/R$ per unit surface stress) with a sufficient resonant frequency. Various structural platforms such as rectangles (with different aspect ratios), square and trapezium (with varying dimensions on one edge) were considered for initial simulation. The simulations were carried out using a computer aided design (CAD) tool, IntelliSuite® (Version 8.7). Based on the initial simulations, a triangular cantilever platform was chosen for our design as it offers high $\psi$ and measurement bandwidth. Further simulations were carried out on the triangular platform by varying the geometry of the cantilever platform and the dimensions of the piezoresistor with surface stress as the mechanical loading. From the simulation results it is demonstrated that the triangular cantilever platform can be considered as the mechanical platform for biochemical sensing applications with an integrated piezoresistor as the readout mechanism.

## 2. Design parameters

A microcantilever with an integrated piezoresistor consists of the following three layers (from the top): (a) an immobilization

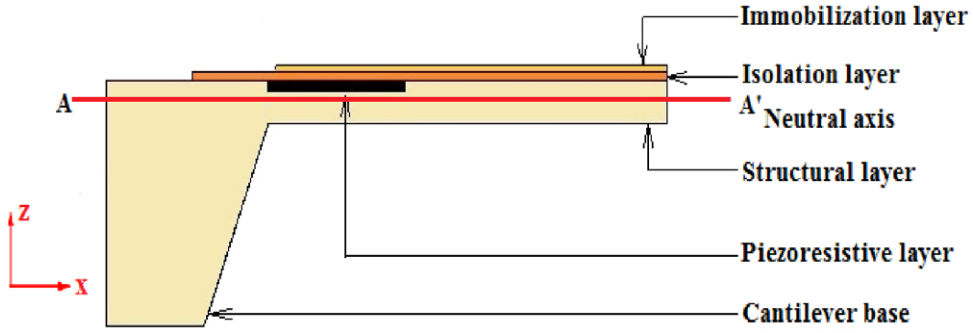


**Figure 1.** A crossectional view of a composite piezoresistive microcantilever biochemical sensor.

layer, (b) an isolation layer, and (c) a structural layer with an embedded piezoresistor. The specific target species to be detected binds to the receptors (species having affinity towards the target molecules) grafted on the immobilization layer of the cantilever. The target-receptor binding either on the top or bottom surface of the cantilever induces a differential stress on the opposite faces, leading to cantilever bending. The voltage or current excited embedded piezoresistor completes the transduction of the induced surface stress into an equivalent electrical signal. The piezoresistor is electrically isolated from the environment by encapsulating it with an isolation layer. The need for an immobilization layer, an embedded piezoresistor and an isolation layer makes the piezoresistive affinity microcantilever sensor a composite structure. Figure 1 shows a crossectional view of a piezoresistive microcantilever composite structure. The microcantilever sensors are designed in (1 0 0) silicon wafers with the cantilever and piezoresistor aligned along the <1 1 0> direction.

The design specifications of the proposed piezoresistive affinity microcantilever sensor for biochemical sensing application are shown in table 1.

Factors that determine the geometrical shape and the dimensions of a piezoresistive microcantilever platform based surface stress sensor are:

- Mechanical sensitivity and stability
  (a) Spring constant
  (b) Resonant frequency
- Electrical sensitivity

The above-mentioned factors are discussed in detail in the following sub-sections

### 2.1. Mechanical sensitivity and stability

The relative change in the cantilever displacement per unit surface stress i.e. the mechanical sensitivity is a function of the material and geometrical parameters of the composite microcantilever platform. The electrical sensitivity denoted as $(\Delta R/R)/\sigma_s$ is the ratio between the change in resistance ($\Delta R$) and the nominal resistance ($R$), which is proportional to the stress induced due to the cantilever bending and hence on the mechanical sensitivity. On the other hand, the cantilever platform should have high immunity against noises such as external vibration. The primary requirement for high noise immunity is a higher resonant frequency ($f_0$) of the cantilever platform. Thus, the composite cantilever is designed to meet contradictory requirements i.e. ($\Delta R/R$) and $f_0$. The product $(\Delta R/R)f_0^2$ is used as a figure of merit (FoM) in designing the cantilever platform.

*2.1.1. Spring constant ($k_s$).* The mechanical displacement sensitivity of the sensor is inversely proportional to the spring constant or the stiffness of the cantilever platform. The spring constant of a composite microcantilever is given by [26]

$$k_S = \frac{C\sum E_i I_i}{l^3} \tag{1}$$

where, $E_i$ represents the Young's modulus of the $i$th layer, $C$ is a constant that depends on the type of mechanical loading, $l$ is the length of the cantilever, and $I_i$ is the moment of inertia of the $i$th layer to the neutral plane of the composite cantilever.

The moment of inertia ($I$) for a generic rectangular composite structure is given by

$$I_i = \frac{wt_i{}^3}{12} + wt_i(Z_i - Z_{\mathrm{N}})^2 \tag{2}$$

where $w$ and $t$ are the width and thickness of the composite cantilever, and the difference $Z_i - Z_{\mathrm{N}}$ shows the distance between the $i$th layer and the neutral plane of the cantilever structure.

Neutral axis (refer to figure 1) of a structure is defined as the plane along which the compressive and the tensile stress tensors are zero. In a composite microcantilever platform, the neutral plane of the structure plays an important role. Specifically, the positioning of the neutral axis by careful design of the composite cantilever layer thicknesses is critical in maximizing the electrical sensitivity. Position of the neutral plane ($Z_{\mathrm{N}}$) in a composite cantilever platform is given by

$$Z_{\mathrm{N}} = \frac{\sum_{i=1}^{n} Z_i E_i t_i}{\sum_{i=1}^{n} E_i t_i} \tag{3}$$

where, $Z_i$ is the position of the center of the $i$th layer from an arbitrary reference.

From the equations (1)–(3), it is evident that the spring constant is a function of the material properties and the dimensions of the constituent layers of a composite cantilever. For the intended application, the spring constant should be low enough to yield a high mechanical and hence electrical sensitivity. At the same time, the spring constant should be high enough for immunity against external environmental noises.

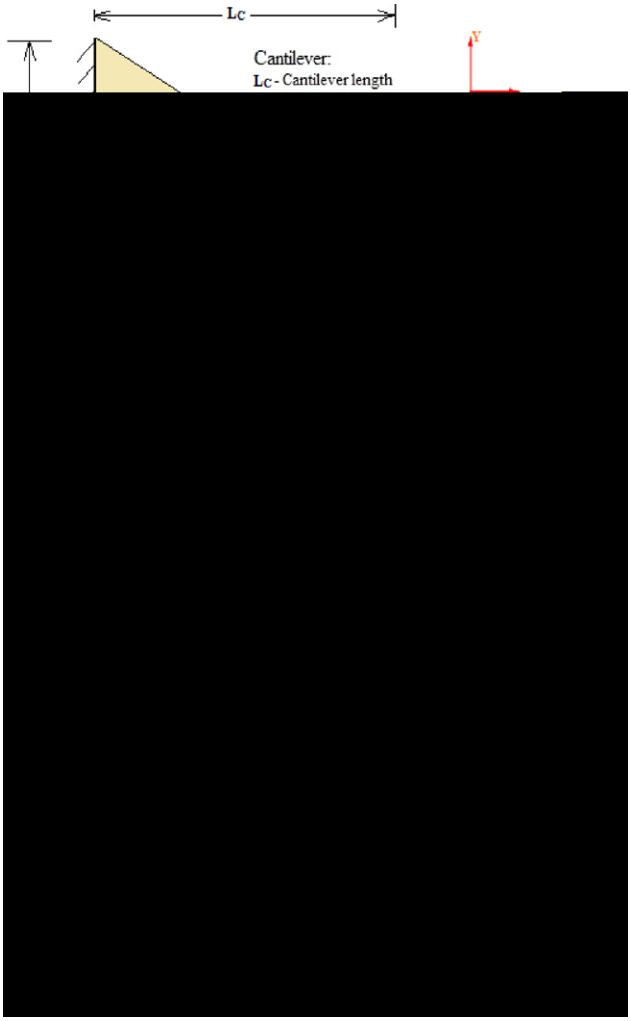


**Figure 2.** (*a*) Triangular cantilever platform with a zoom in view of the piezoresistor, (*b*) different cantilever platform geometries (i) rectangle-1 with aspect ratio (*L*/*W*) more than unity; (ii) square; (iii) rectangle-2 with aspect ratio (*L*/*W*) < 1; (iv) trapezoidal.

*2.1.2. Resonant frequency ($f_n$).* The resonant frequency of a composite microcantilever is given by [26]

$$f_n = \frac{1}{2\pi}\frac{{v_n}^2}{l^2}\sqrt{\frac{1}{m}\sum_{i=1}^{n} E_i I_i} \tag{4}$$

where, $f_n$ and $v_n$ are the $n$th resonant frequency and its corresponding dimensionless eigen value ($v_1 = 1.875$) respectively. Mass $m$ of the composite cantilever can be obtained by the relationship, $m = lw\sum_{i=1}^{n} \rho_i t_i$, where $\rho_i$ is the density of the $i$th layer. For a mechanically stable response, the measurement bandwidth of a cantilever sensor is generally chosen as half of the resonant frequency of the structure [26]. In the present work, the composite cantilever is designed for a resonant frequency more than 25 kHz so as to suppress external noises, mainly vibration noise.

### 2.2. Electrical sensitivity

For a surface stress based piezoresistive microcantilever sensor, maximum electrical sensitivity is obtained when the difference between the longitudinal and the transverse stress is maximum, given by

$$\frac{\Delta R}{R} = \pi_X(\sigma_l - \sigma_t) \tag{5}$$

where, $\Delta R/R$ is the relative change in resistance of the piezoresistor due to the target-receptor interaction, $\sigma_l$ & $\sigma_t$ are the longitudinal and transverse stress components, and the piezoresistive coefficient $\pi_X \approx \pi_{44}/2$ for a $p$-type piezoresistor aligned along the <1 1 0> direction.

With an applied surface stress as a mechanical loading, the spatial variation of the deflection induced stress on the cantilever comprises of both the longitudinal and the transverse stress unlike the AFM cantilever where the mechanical loading (a concentrated point load at the tip) induces the stress dominant in the longitudinal direction [27]. The 2D nature of the stress profile in the case of a surface stress loading plays a crucial role in determining the cantilever geometry and dimensions, and in turn maximizing the electrical sensitivity. Moreover, for a doped $p$-type SCS (single crystal silicon) piezoresistor, the longitudinal and transverse piezoresistive coefficients are comparable in magnitude with the opposite sign [28]. Hence, it is important to consider the effect of the transverse stress on the electrical sensitivity.

The electrical sensitivity for a surface stress based sensor with mechanical loading at the top of the cantilever is given by [29]

$$\frac{\left(\frac{\Delta R}{R}\right)}{\sigma_S} = -G\frac{Z_T\left(Z_T - \sum_{j=0}^{R} t_j + \frac{t_R}{2}\right)}{\sum_i E_i t_i\left(\left(Z_T - \sum_{j=0}^{i} t_j + \frac{t_i}{2}\right)^2 + \frac{1}{3}\left(\frac{t_i}{2}\right)^2\right)} - G\frac{1}{\sum_i E_i t_i} \tag{6}$$

where $G$ represents the gauge factor of the piezoresistor, $Z_T$ is the position of the top surface layer with respect to the neutral axis, $t_i$ is the thickness of the $i$th layer, $j{:}0 \rightarrow R$ depicts the variation from the top of the cantilever platform to bottom of the piezoresistor, $j{:}0 \rightarrow i$ depicts the variation from the top of the cantilever platform to the bottom of the $i$th layer, $R$ is the piezoresistor layer and $t_R$ represents the thickness of the piezoresistor layer.

For a constant length and width of the cantilever, surface stress sensitivity is a function of the gauge factor, the material properties and the thickness of each constituent layer of the composite cantilever. Electrical sensitivity can be maximized by selecting a piezoresistor with high gauge factor like SCS over metals or polycrystalline silicon. Electrical sensitivity can further be improved by maximizing the difference between the neutral plane of the cantilever and mid-plane of the piezoresistor as evident from equation (6).

In summary, both the electrical sensitivity and the mechanical stability of a piezoresistive affinity microcantilever sensor are functions of cantilever dimensions and material properties.

**Table 2.** Microscale material properties used in the simulations [37, 38].

| Electrical and mechanical parameters | Silicon | Boron doped silicon | Silicon dioxide | Gold |
|---|---|---|---|---|
| Young's modulus, E (GPa) | 169 | 169 | 70 | 75 |
| Poisson's ratio | 0.064 | 0.064 | 0.20 | 0.42 |
| Density ($g\,cm^{-3}$) | 2.32 | 2.32 | 2.22 | 19.3 |
| Piezoresistive coefficient, $\pi_{44}$(1/MPa) for a doping of 5E19 ($cm^{-3}$) [39] | — | 78E-5 | — | — |

A trade-off has to be made between the electrical sensitivity and the mechanical stability while deciding the total thickness of the cantilever. With immunity from external noises, electrical sensitivity can further be improved by sensitivity enhancement techniques like stress concentration methods [30] and dimensional optimization of the piezoresistor and the cantilever [31].

## 3. Simulation environment and design methodology

The initial cantilever design for choosing the shape and dimensions of the cantilever platform for biochemical sensing applications is governed by the mentioned equations (1)–(6). In the present study, various modules of a Finite Element Method (FEM) based CAD tool IntelliSuite® (Version 8.7) are used for designing the microcantilever sensor. The process modeling and the virtual fabrication of the composite microcantilever is performed in IntelliFAB® process simulation module. The static, dynamic and electrical characteristics of the piezoresistive microcantilever sensor are analyzed in the Thermo-Electro-Mechanical® (TEM) module. The composite microcantilever structure was meshed in the Hexpresso® module that utilizes 20-node brick parabolic element meshing (isotropic) for the electro-mechanical analysis of the structure. The modeling approach and the mesh optimization of the structures were validated by comparing its electrical sensitivity with the reported piezoresistive cantilever sensors in [40]. Mesh elements with a minimum mesh size of less than 2 $\mu$m were taken for numerical simulations to optimize the computational accuracy in determining the electrical and mechanical sensitivity of the sensor and the computation time.

The thicknesses of the isolation and the immobilization layers are chosen based on the reported values in the literature [32]. The doping of a *p*-type SCS piezoresistor can range from 1E16 to 1E21 $cm^{-3}$, however the choice of doping is a tradeoff between electrical sensitivity, temperature coefficient of piezoresistivity (TCP) and fabrication of a stable ohmic contact. Below 1E17 $cm^{-3}$ it is difficult to fabricate stable ohmic contacts [33, 34] and above 1E20 $cm^{-3}$ the piezoresistive coefficients are too low. The rationale for choosing 5E19 $cm^{-3}$ as the doping concentration is the reduced effect of temperature drift due to lower TCP at higher doping levels [35]. The effect of higher doping on SNR can further be improved by subsequent signal processing stages.

**Table 3.** Dimensional details of the composite cantilever.

| Parameter | Value |
|---|---|
| Thickness of structural Si layer | 500 nm |
| Thickness of isolation $SiO_2$ layer | 75 nm |
| Thickness of immobilization Au layer | 50 nm |
| Junction depth of the boron doped piezoresistor | 100 nm |
| Total composite cantilever thickness | 625 nm |

The u-shaped piezoresistor is placed at the central region near the base of the cantilever where the stress is maximum. The piezoresistor dimensions are $W_S = W_T = 20\,\mu$m, $W_P = 60\,\mu$m, and $L_P = 40\,\mu$m except for the rectangle-1 cantilever as shown in figure 2. For electrical analysis, the doping concentration and the thickness of the piezoresistor are fixed at 5E19 $cm^{-3}$ and 100 nm respectively. The material properties and the dimensional details of the initial design of the composite cantilever are summarized in tables 2 and 3 respectively. The individual piezoresistor element is excited with a voltage of 5 V. Simulations are performed for a surface stress in the range of 0–100 E-3 $N\,m^{-1}$ which are typical in the case of biochemical interactions on an immobilization surface [36].

## 4. Results and discussion

### *4.1. Selection of cantilever platform geometry*

Preliminary simulations were carried out with different cantilever platforms such as rectangle, triangle, square and trapezoid as shown in figure 2. Two configurations of rectangular cantilever ($L/W > 1$ and $L/W < 1$) and five configurations of trapezoid cantilever (by varying the dimension of one edge) along with a triangle and a square shaped cantilever platform resulted in a total of nine test structures from four shapes.

In the preliminary simulation phase, a common cantilever width of 200 $\mu$m is fixed for all the configurations (except for rectangular-1) as shown in figure 2. Maximum displacement induced Mises stress, resonant frequency and electrical sensitivity of all the structures were found out using various modules of the CAD tool and the results are given in table 4. Rectangle-1 ($L/W > 1$), the most generic cantilever platform, is best suited for point load or force sensing applications rather than surface stress sensing [40]. The results also reconfirm that the slender beam structure is suited for point load sensing since the factor $\psi$ is least for rectangle-1

**Table 4.** Performance comparison of different cantilever platforms (geometries in figure 2).

| Cantilever type (Geometry) | Dimensional details of cantilever ($\mu$m) | Maximum mises stress (MPa) | Maximum tip displacement ($Z$) ($\mu$m) | $\Delta R/R$ (E-4) | Electrical sensitivity $(\Delta R/R)/\sigma_s$ E-2 ($m N^{-1}$) | Resonant frequency ($f_0$) (kHz) | $(\Delta R/R)f_0^2$ E3 $(Hz)^2$ |
|---|---|---|---|---|---|---|---|
| Rectangle 1 ($L/W > 1$) | $L = 200$, $W = 100$ $L1 = 160$, $W_S = 10$ | 14.1285 | 2.5838 | 4.7130 | 4.7130 | 19.9179 | 186.9754 |
| Rectangle 2 ($L/W < 1$) | $L = 100$, $W = 200$ | 3.2766 | 0.1588 | 1.7868 | 1.7868 | 79.7116 | 1135.3218 |
| Triangle | $L = W = 200$ | 5.4880 | 0.9204 | 2.8592 | 2.8592 | 34.0421 | 331.3425 |
| Trapezoid-1 | $L = W = 200$, w1= 20 | 6.4822 | 1.1433 | 3.3757 | 3.3757 | 27.7923 | 260.7430 |
| Trapezoid-2 | $L = W = 200$, w1= 40 | 7.4300 | 1.3448 | 3.8524 | 3.8524 | 25.8508 | 257.4419 |
| Trapezoid-3 | $L = W = 200$, w1= 80 | 9.1927 | 1.7020 | 4.7664 | 4.7664 | 21.1962 | 214.1442 |
| Trapezoid-4 | $L = W$ =200, w1= 120 | 10.7940 | 2.0152 | 5.6408 | 5.6408 | 19.1108 | 206.0148 |
| Trapezoid-5 | $L = W = 200$, w1= 160 | 12.2560 | 2.2971 | 6.4358 | 6.4358 | 17.6685 | 200.9101 |
| Square | $L = W = 200$ | 13.6313 | 2.5559 | 7.2310 | 7.2310 | 16.6322 | 200.0312 |

[a] Values computed at an applied surface stress, $\sigma_s$ = 10E-3 N $m^{-1}$, thickness of the composite cantilever = 625 nm.

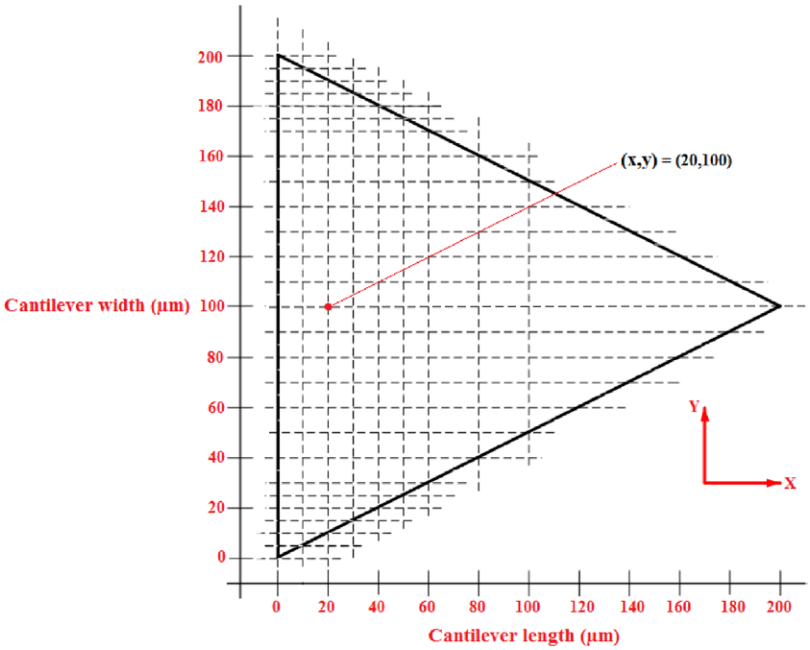


**Figure 3.** Blueprint for analyzing the stress profile in the triangular cantilever.

($L/W > 1$) compared to all other structures considered here. It is observed that the magnitude of the maximum Mises stress generated in the triangular cantilever platform is 67.49% higher than that of the rectangular-2 ($L/W < 1$) cantilever platform. Also, the resonant frequency of the triangular cantilever is higher compared to the square and the trapezoid (all five configurations) cantilever platforms i.e. it has a higher bandwidth of measurement. Moreover, the triangular shape microcantilever platform has the advantage of a larger torsional stiffness [41]. A relatively larger value of torsional stiffness minimizes the rotation of the composite cantilever leading to a reduced structural nonlinearity against the large deflection of the cantilever. To summarize, the triangular cantilever platform for piezoresistive bio-chemical sensing has the following advantages:

- A relatively higher $\psi$
- High measurement bandwidth i.e. a higher range of mechanically stable responses
- Resistance against large deflection induced nonlinearities

From table 4 it is evident that out of nine test structures, $\psi$ of rectangle-2 ($L/W < 1$) is maximum mainly due to its high resonant frequency, since $\psi$ is proportional to the square of the resonant frequency; however the $\Delta R/R$ of the triangular structure is 60.01% higher than rectangle-2 for the same cantilever area, with fixed piezoresistor geometrical and process parameters. Therefore in the present study, the triangular platform is considered as an alternative geometry for affinity microcantilever sensors with piezoresistive readout. Further investigations were carried out on the triangular cantilever platform to evaluate its performance by varying, (a) geometrical dimensions of the cantilever, (b) piezoresistor junction depth, and (c) the relative dimensions of the cantilever and the piezoresistor. The results are discussed in the subsequent sections.

### 4.2. Simulation results of triangular cantilever platform

*4.2.1. Stress profile simulation.* Stress profile analysis is essential to comprehending the spatial variation of the 2D stress generated on the cantilever platform due to the surface stress loading. The nature of the 2D stress is of prime importance, considering its implications to locate the position of the piezoresistor in the triangular cantilever platform. A blueprint shown in figure 3 is considered for analyzing the spatial variation of stress tensors ($\sigma_{XX}$ & $\sigma_{YY}$) on the cantilever surface. A Cartesian coordinate system is utilized to represent specific numerical coordinates on the cantilever platform surface. Numerical simulations were performed by applying surface stress loading of 10 E-3 N m$^{-1}$, with 115 test points for observing the stress generated on the cantilever platform. The induced stress is 3D in nature with variations along the $X$, $Y$ and $Z$-axes. However, for the designed cantilever and piezoresistor dimensions, the stress magnitude variation along the thickness of the thin piezoresistor is assumed to be constant compared to the entire cantilever thickness. It is indeed understood from equation (5) that the piezoresistor should be located where the difference between the longitudinal ($\sigma_{XX}$) and the transverse ($\sigma_{YY}$) stress tensor is maximum in order to obtain maximum electrical sensitivity. It is evident from figures 4($a$) and ($b$) that the stress tensor along the $X$-axis is maximum at the central base region and its magnitude decreases as we move away towards the edges along the width and towards the length of the cantilever platform. A similar pattern of the stress tensor along the $Y$-axis is shown in figures 4($c$) and ($d$). The factor $\sigma_0 = \sigma_{XX} - \sigma_{YY}$, is calculated and its variation along the cantilever length and width is represented graphically in figure 4($e$). It is found that the difference of the longitudinal and the transverse stress component is maximum near the central region at (0, 100) $\mu$m of the cantilever platform. Its magnitude falls by 40% and 96.87% at (0, 20) $\mu$m and (0, 0) $\mu$m respectively. Similarly, the magnitude of $\sigma_0$ decreases by 44.8% at (50, 100) $\mu$m. Hence, for placing the piezoresistor we have considered the central base region of length 40 $\mu$m and width 60 $\mu$m spanning around the cantilever width of 100 $\mu$m at the base.

*4.2.2. Variation in the cantilever dimensions.* The dimensions of the cantilever platform are a tradeoff between the electrical sensitivity and the mechanical parameters like spring constant, resonant frequency etc as evident from the equations (1)–(6) presented in section 2. In the following sections the length, width and thickness of the triangular cantilever platform are optimized with respect to the resonant frequency, spring constant and electrical sensitivity for fixed piezoresistor dimensions.

*4.2.2.1 Effect of cantilever length.* With the width and the thickness of the cantilever fixed, as the longitudinal dimensions of the cantilever is increased, there is an increase in the compliance of the cantilever to bend due to a reduction in the spring constant (in accordance to the equation (1)). An increase in the cantilever bending leads to an increase in the magnitude of the stress experienced by the piezoresistor. The higher stress gauged by the piezoresistor is transduced into a higher electrical sensitivity. For instance, as shown in figure 5, when the cantilever length is increased from 60 to 220 $\mu$m, electrical sensitivity increases by 10.25 times, however, at the same time the FOM ($\psi$) of the sensor reduces by 12.92 times. This reduction in the magnitude of $\psi$ with an increase in the cantilever length can be attributed due to the reduction in the resonant frequency of the cantilever platform. Hence, it is evident that the shorter cantilever platforms are more suitable for surface stress sensing applications.

*4.2.2.2 Effect of cantilever width.* The electrical sensitivity is a function of the piezoresistive coefficient ($\pi_X$), the longitudinal ($\sigma_{XX}$) and the transverse ($\sigma_{YY}$) stress components related by equation (5). The piezoresistive coefficient is fixed for a given dopant and doping concentration hence electrical sensitivity can only be enhanced by maximizing the difference between the two stress tensors. The transverse dimension of the cantilever platform plays a critical role in determining the magnitude and the spatial profile of the induced stress on the cantilever surface. The parameter $\sigma_0$ represents the maximum difference in magnitude of the longitudinal and the transverse stress tensors ($\sigma_{XX} - \sigma_{YY}$) in the triangular cantilever platform under mechanical loading. Simulation results (figure 6) show the effect of the variation in the cantilever width on $\sigma_0$ for a given surface stress loading and its relative influence on the electrical sensitivity. As evident, an increase in the cantilever transverse dimension from 100 to 400 $\mu$m results in an increase of $\sigma_0$ by 27.08%. The increase in the magnitude of $\sigma_0$ in turn leads to an increment in electrical sensitivity by 32.82% (in accordance with equation (5)). Hence, as the width of the cantilever platform increases, the parameter $\sigma_0$ also increases, therefore for surface stress sensing a wider cantilever is preferred.

*4.2.2.3 Effect of cantilever thickness.* The electrical sensitivity is a function of the position of the piezoresistor with respect to the neutral axis of the composite structure (equation (6)). The dimensional optimization especially the thickness of the different constituent layers of the composite cantilever plays a crucial role in determining the position of the neutral axis. Hence, we have fixed the thickness of the isolation and the immobilization layers for the simulation analysis. The focus is on optimizing the thickness of the structural layer to

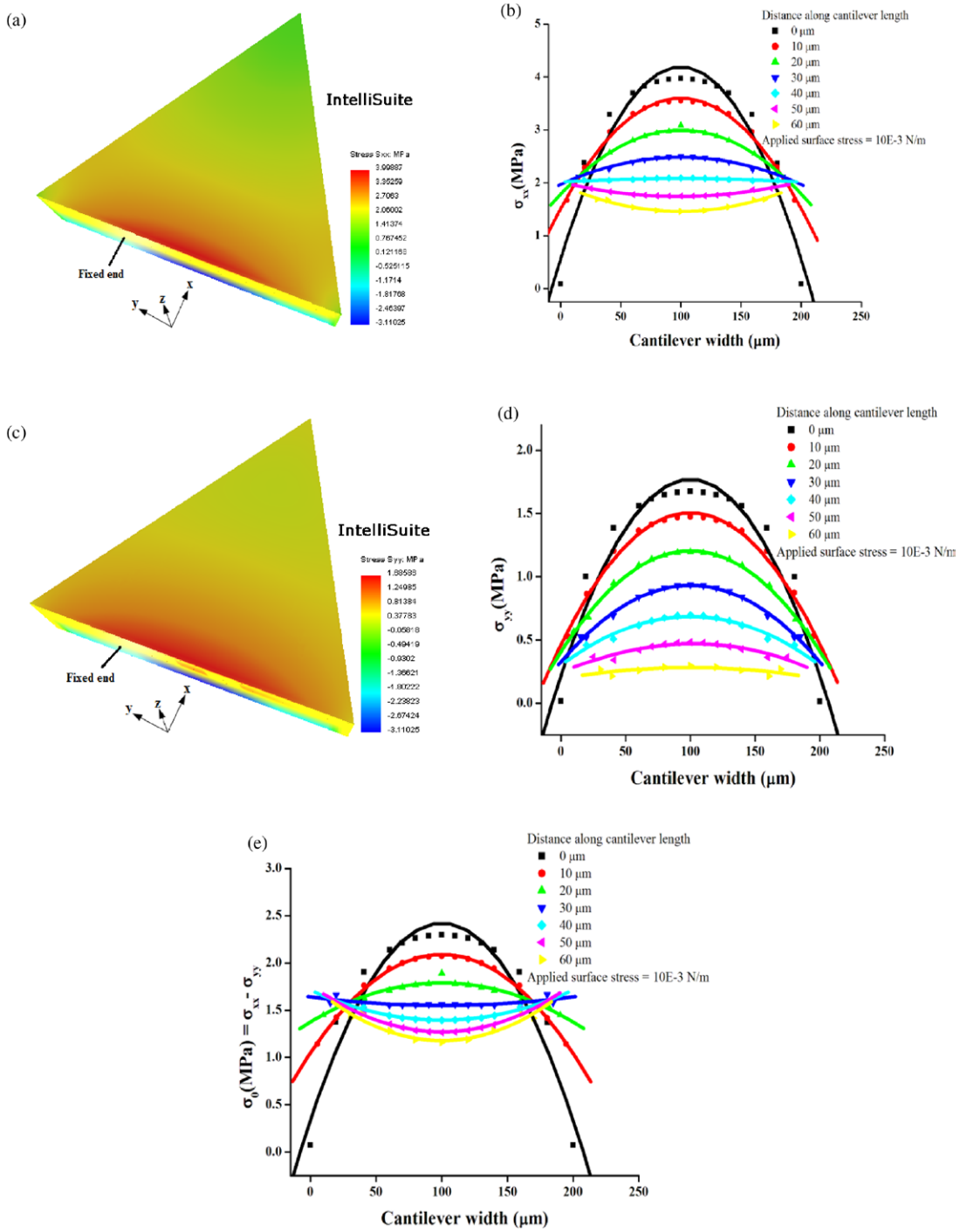


**Figure 4.** (*a*) Stress profile of longitudinal stress ($\sigma_{XX}$) in the triangular cantilever platform. (*b*) Graphical representation of longitudinal stress profile ($\sigma_{XX}$) in the triangular cantilever platform. (*c*) Stress profile of transverse stress ($\sigma_{YY}$) in the triangular cantilever platform. (*d*) Graphical representation of transverse stress ($\sigma_{YY}$) in the triangular cantilever platform. (*e*) Graphical representation of the difference in the longitudinal and transverse stress tensor in the triangular cantilever platform.

maximize the electrical sensitivity. The maximum electrical sensitivity is obtained at an optimum structural layer thickness where the difference between the cantilever neutral axis and the mid-plane of the piezoresistor is maximum. However, after a certain optimal structural layer thickness, the effect of increasing the difference between the position of the piezoresistor and the neutral axis is nullified by the decrease in the cantilever bending due to the increased stiffness of the structure. This increase in the stiffness of the cantilever leads to a reduction in the magnitude of stress experienced by the piezoresistor resulting in a reduced electrical sensitivity. From figure 7, with the increase in the structural layer thickness from 300 to 800 nm, the cantilever tip displacement decreases by 7.85 times. Initially, the electrical sensitivity increases when the structural layer thickness is increased from 300 to 500 nm due to the increase in the difference of the position of

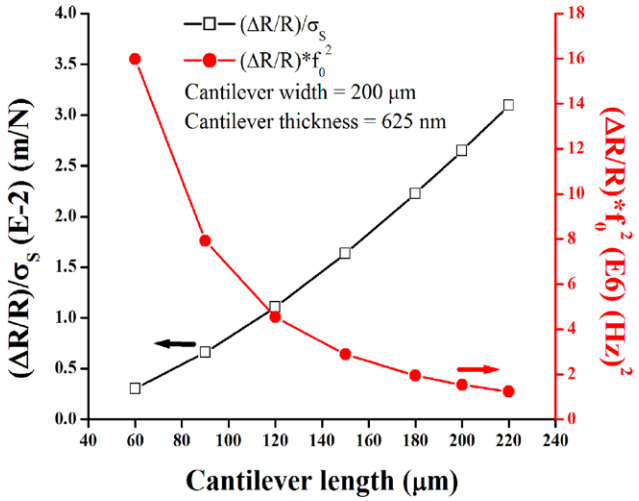


**Figure 5.** Variation in the electrical sensitivity and the resonant frequency versus cantilever length.

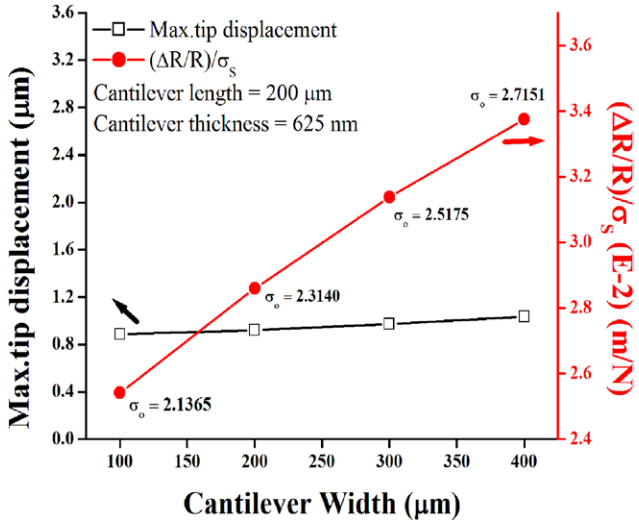


**Figure 6.** Variation in the electrical sensitivity and the displacement of the cantilever tip versus cantilever width.

the piezoresistor and the neutral axis. The value of electrical sensitivity peaks at an optimal structural layer thickness of 500 nm. However, electrical sensitivity then falls by 18% as the cantilever structural layer thickness is increased to 800 nm due to an increase in the stiffness of the multilayer structure.

*4.2.3. Variation in the piezoresistor dimensions.* To satisfy the competing design specifications of the spring constant, resonant frequency and electrical sensitivity, from the previous analysis we have chosen the cantilever dimensions as: $L = W = 200\,\mu$m and $t_{\text{total}} = 625$ nm (with $t_{\text{structure}} = 500$ nm). In this section, a detailed dimensional analysis of the electrically active piezoresistor on the electrical sensitivity is carried out, considering the influence of the cantilever dimensions. The surface doping concentration and the initial dimensions of the piezoresistor are chosen to satisfy the competing factors such as the magnitude of piezoresistive coefficient, fabrication of a stable ohmic contact, and interfacing of the sensor with the

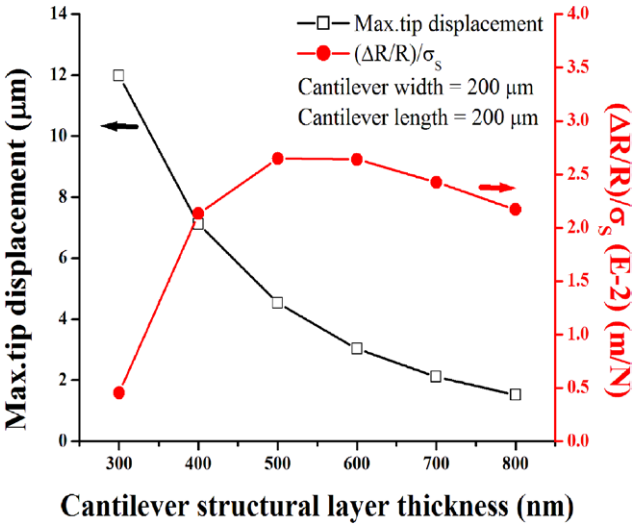


**Figure 7.** Variation in the electrical sensitivity and the displacement of the cantilever tip versus cantilever structural layer thickness.

subsequent signal processing circuitry (especially the instrumentation amplifier). Taking into account the aforementioned parameters the resistance of the piezoresistor is limited to a few kilo-ohms [18]. The dimensional details of the piezoresistor chosen for simulations are: $L_{\text{P}} = 40\,\mu$m, $W_{\text{P}} = 60\,\mu$m, $W_{\text{T}} = 20\,\mu$m, and $W_{\text{S}} = 20\,\mu$m (refer figure 2). All simulations are performed with a fixed surface doping concentration, and it is assumed that the doping profile is uniform throughout the thickness of the piezoresistor. In the following sections, a systematic analysis is performed to comprehend the relative influence of the piezoresistor dimensions with respect to the cantilever on the electrical sensitivity.

*4.2.3.1 Effect of piezoresistor junction depth on electrical sensitivity.* The magnitude of the generated stress on the cantilever platform due to the mechanical loading is more dominant near the cantilever surface and it decreases as we move towards the neutral axis of the cantilever. As shown in figure 8, as the junction depth of the piezoresistor is varied from 50 to 250 nm on a silicon structural layer of 500 nm thickness, the electrical sensitivity decreases by 91.1%. Hence, for a piezoresistive cantilever sensor the junction depth of the doped or implanted resistor should be as closer to the surface of the cantilever to maximize the electrical sensitivity. Factors that limit the thickness of the piezoresistive layer are the technology related constraints, mainly the doping method and the required nominal resistance.

*4.2.3.2 Effect of piezoresistor to cantilever length ratio ($\alpha = L_{Piezo}/L_{Cantilever}$) on electrical sensitivity.* From figure 9, it is evident that as the piezoresistor to cantilever length ratio approaches unity i.e. as the piezoresistor extends more towards the tip of the cantilever, the electrical sensitivity decreases. The decrease in electrical sensitivity is attributed to the fact that the maximum stress difference ($\sigma_{XX} - \sigma_{YY}$) exists near the central base region of the cantilever's fixed end and its magnitude decreases as we move towards the tip of the cantilever as explained in section 4.2.1, figure 4(*e*). Moreover,

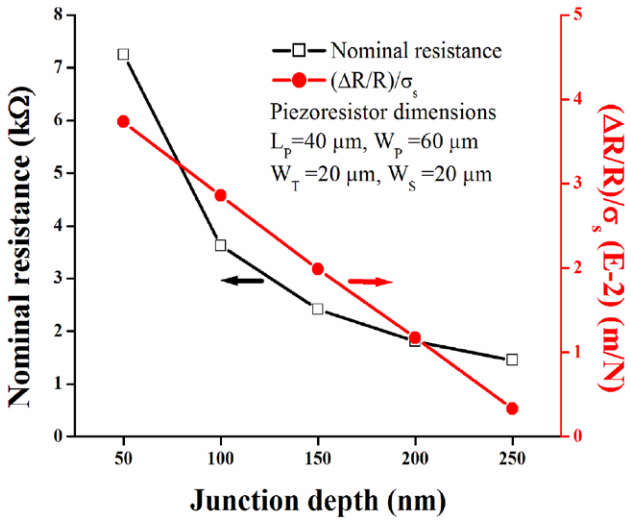


**Figure 8.** Variation in the electrical sensitivity and the nominal resistance versus the junction depth of the piezoresistor for fixed cantilever dimensions.

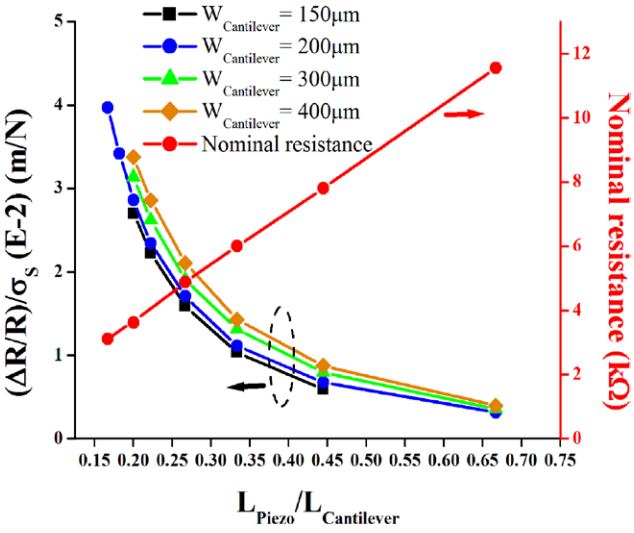


**Figure 9.** Variation in the electrical sensitivity and the nominal resistance versus ratio of the piezoresistor to cantilever length for different cantilever widths.

the unstrained resistance i.e. the resistance unaffected by the stress increases as $\alpha$ approaches unity leading to a decrease in the electrical sensitivity. For instance, in the case of the cantilever with width $W = 200\,\mu$m, when $\alpha$ increases from 0.16 to 0.66 with an increase in the nominal resistance by 3.7 times, the electrical sensitivity decreases by 91.95%. A wider cantilever shows higher sensitivity due to an increase in the difference in the longitudinal and the transverse stress, reconfirming the result in figure 6. For instance at $\alpha = 0.33$ the electrical sensitivity of a 400 $\mu$m wide cantilever is 38.46% more than that of a 150 $\mu$m wide cantilever.

*4.2.3.3 Effect of piezoresistor to cantilever width ratio ($\beta = W_{Piezo}/W_{Cantilever}$) on electrical sensitivity.* The effect of $\beta$ (where, $W_{Piezo} = (W_P - W_S)/2$) variation on the electrical sensitivity is plotted in figure 10 for different cantilever width.

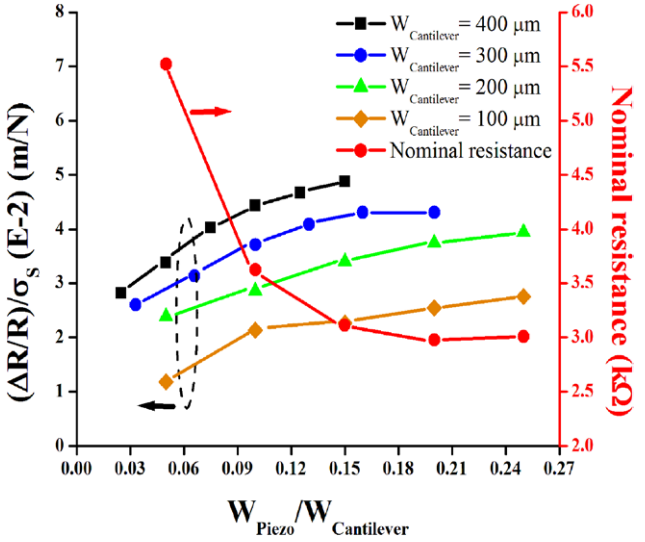


**Figure 10.** Variation in the electrical sensitivity and the nominal resistance versus ratio of the piezoresistor to cantilever width for different cantilever width.

From figure 10, it is evident that as the piezoresistor width increases, there is an increase in the electrical sensitivity of the piezoresistive cantilever sensor. For example, in the case of cantilever with base width 200 $\mu$m, as the piezoresistor width increases from 10 $\mu$m to 50 $\mu$m (the nominal resistance decreases by 45.3%) there is an increase in the electrical sensitivity by 65.24%. The increase in the electrical sensitivity can be attributed to the increase in the number of charge carriers due to an increase in the volume of the piezoresistor. The increase in the electrical sensitivity with an increase in $\beta$ can also be attributed to the fact that, in a cantilever platform with a unity aspect, the surface stress loading induces a stress profile more concentrated near the fixed base and distributed towards the transverse direction, hence a wider piezoresistive element gauges the stress better. It is also observed that as the cantilever becomes wider, there is an increase in the electrical sensitivity. For instance, at $\beta = 0.15$, the electrical sensitivity of a 400 $\mu$m wide cantilever is 4.87 E-2 which is 2.15 times more than the electrical sensitivity (2.26 E-2) of a cantilever with a base width of 100 $\mu$m. Moreover, a wider cantilever should be the optimal design, since the area available for immobilization of receptors will be more, leading to a higher biological sensitivity.

*4.2.3.4 Effect of piezoresistor to cantilever thickness ratio ($\gamma = T_{Piezo}/T_{Cantilever}$) on electrical sensitivity.* The profound effect of $\gamma$ on the electrical sensitivity is depicted in table 5 with its corresponding inset figures. According to equation (6) maximum electrical sensitivity is a compromise between two competing parameters, first the difference between the neutral axis of the cantilever and the mid-plane of the piezoresistor ($Z_N - Z_R$) and second, the flexural rigidity of the cantilever platform. Both the parameters depend on the dimensional aspects especially the thickness of the constituent layers and the material properties like the Young's modulus. However, due to the complexity of equation (6), the dependence of the electrical sensitivity on the governing

**Table 5.** Effect of piezoresistor to cantilever thickness ratio on electrical sensitivity.

| Thickness of the piezoresistor | Parameters | | | | | | | | |
|---|---|---|---|---|---|---|---|---|---|
| | $T_{Canti,\,str}$ (nm) | $T_{piezo}/T_{Canti,str}$ | $Z_N - Z_R$ ($\mu$m) | % change in $Z_N - Z_R$ | $k$ (N m$^{-1}$) | % change in $k$ | Slope | $(\Delta R/R)/\sigma_s$ (E-2) | Plot |
| $T_{piezo} = 50$ nm | 300 | 0.16 | 125 | — | 0.7935 | — | | 2.8592 | |
| | 400 | 0.12 | 175 | 40 | 1.3562 | 70.91 | | 3.8127 | |
| | 500 | 0.1 | 225 | 80 | 2.1661 | 172.98 | | 3.7332 | |
| | 600 | 0.083 | 275 | 120 | 3.2707 | 312.18 | | 3.2565 | |
| | 700 | 0.071 | 325 | 160 | 4.7186 | 494.65 | | 2.8592 | |
| | 800 | 0.0625 | 375 | 200 | 6.5584 | 726.51 | | 2.4620 | |
| $T_{piezo} = 150$ nm | 400 | 0.375 | 125 | — | 1.3560 | — | | 1.1382 | |
| | 500 | 0.3 | 175 | 40 | 2.1657 | 59.71 | | 1.9853 | |
| | 600 | 0.25 | 225 | 80 | 3.2702 | 141.16 | | 2.1707 | |
| | 700 | 0.214 | 275 | 120 | 4.7179 | 247.92 | | 2.0648 | |
| | 800 | 0.187 | 325 | 160 | 6.5575 | 383.59 | | 1.9060 | |
| | 900 | 0.166 | 375 | 200 | 8.8377 | 551.74 | | 1.7206 | |
| $T_{piezo} = 250$ nm | 500 | 0.5 | 125 | — | 2.1655 | — | | 0.3334 | |
| | 600 | 0.416 | 175 | 40 | 3.2700 | 51.00 | | 1.0640 | |
| | 700 | 0.357 | 225 | 80 | 4.7175 | 117.84 | | 1.3182 | |
| | 800 | 0.3125 | 275 | 120 | 6.3799 | 194.61 | | 1.3499 | |
| | 900 | 0.277 | 325 | 160 | 8.8367 | 308.06 | | 1.3023 | |
| | 1000 | 0.250 | 375 | 200 | 11.6058 | 435.94 | | 1.2228 | |

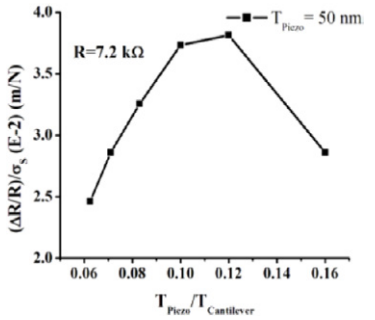


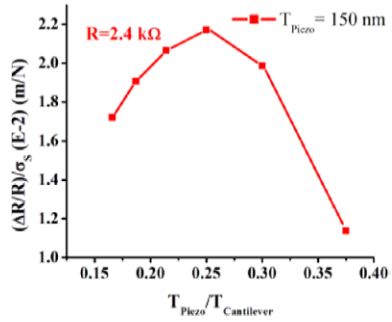


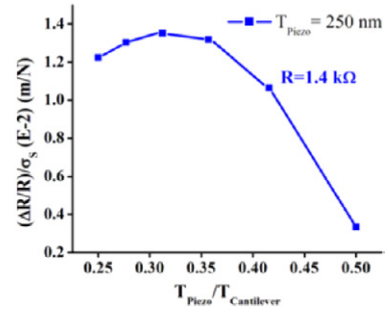

parameters can be better understood by considering only the structural layer thickness with the doped piezoresistor. It can be observed from equation (6) that, when the piezoresistor is infinitely thin compared to the structural layer thickness, equation (6) reduces to

$$\frac{(\Delta R/R)}{\sigma_S} = -4G\frac{1}{E_s t_S} \tag{7}$$

From the above equation it is understood that, for a fixed thickness of the structural layer ($t_s$), the electrical sensitivity is a function of the ratio of the gauge factor ($G$) of the piezoresistor to the Young's modulus of the structural layer ($E_s$). It is evident that, with the increase in the structural layer thickness, the magnitude of the electrical sensitivity will reduce. However, even for small values of the piezoresistor thickness $t_R$ (i.e. when $t_R \neq 0$), the numerator in equation (6) will contribute significantly to the electrical sensitivity by determining the parameter $(Z_N - Z_R)$, where, $Z_R = \sum_{j=0}^{R} t_j - t_R/2$.

Similar dependency can be observed in the case when the thickness of the structural layer is reduced to the thickness of the piezoresistor, i.e. $t_s = 0$. In this case equation (6) reduces to

$$\frac{(\Delta R/R)}{\sigma_S} = -G\frac{1}{E_R t_R} \tag{8}$$

Again, from the above equation it is understood that, for a fixed piezoresistor thickness, the electrical sensitivity is a function of the ratio of the gauge factor ($G$) of the piezoresistor to the Young's modulus of the piezoresistor material ($E_R$). However, for even small values of $t_s$ (i.e. when $t_s \neq 0$), the first term in equation (6) will contribute to the electrical sensitivity.

It is very difficult to understand the effects of governing parameters of equation (6) especially when $t_R \neq 0$ and $t_s \neq 0$. Here, we have computed the values of the parameter $(Z_N - Z_R)$, the spring constant and the electrical sensitivity for three different values of $T_{piezo}$ for $T_{cantilever}$ ranging from 300 nm to 1000 nm, and the results are provided in table 5. The last column of the table 5 represents the corresponding figures. The changes in the slope of the graphs of the last column of table 5, are easily understood by observing the values of $\Delta R/R$ in table 5. For instance, from table 5 when $T_{piezo} = 150$ nm, with the increase in the structural layer thickness from 400 nm to 600 nm, the difference $Z_N - Z_R$ increases by 80% translating in a increase in the electrical sensitivity by 90.71%. However, when the structural layer thickness is increased beyond 600 nm, the increase in the stiffness of the cantilever reduces the cantilever bending resulting in a reduction in the electrical sensitivity. This is evident as the structural layer thickness is increased from 600 nm to 900 nm, the stiffness of the cantilever increases by 170.24%, whereas, $Z_N - Z_R$ increases only by 66.66%. The increased flexural rigidity dominates the incremental change in the parameter $Z_N - Z_R$, hence, the electrical sensitivity is reduced by 20.73%. Similarly, dependence of the electrical sensitivity on the difference between the parameter $Z_N - Z_R$ and the stiffness can be observed in figure 7.

To summarize, we provide a set of design guidelines for the multivariate problem to choose the geometry of a triangular microcantilever sensor with an integrated piezoresistor:

(a) Determination of cantilever length is a tradeoff between the resonant frequency and the electrical sensitivity. A sufficient resonant frequency and spring constant should be designed by scaling the length to ensure stability.
(b) The ratio of $L_{Piezo}/L_{Cantilever}$ should be less than 0.35, i.e. the longitudinal dimension of the piezoresistor should not exceed 35% of the length of the cantilever.
(c) Simulation results show that a shorter and wider cantilever is more suitable for surface stress sensing application. A cantilever with a larger width gives higher electrical sensitivity due to the increase in the factor $\sigma_0 = \sigma_{XX} - \sigma_{YY}$.
(d) An increase in the $W_{Piezo}/W_{Cantilever}$ ratio improves the electrical sensitivity.
(e) Maximizing the electrical sensitivity by optimization of the cantilever thickness is a tradeoff between the parameter $(Z_R - Z_N)$ and the stiffness of the cantilever platform.
(f) A thin piezoresistor close to the surface and the $T_{Piezo}/T_{Cantilever}$ ratio of less than 0.30 is essential for a high electrical sensitivity.

## 5. Conclusions

This paper comprehends the design of a triangular cantilever platform affinity biochemical sensor with an integrated piezoresistor based on the analytical equations and numerical simulations. A systematic study was carried out for the selection of the cantilever platform's shape based on the FoM, $\psi = (\Delta R/R)f_0^2$ and the constraints imposed by the competing factors of electrical sensitivity and mechanical stability. The triangular cantilever platform was illustrated to have a better performance in terms of the aforementioned parameters compared to the other cantilever platforms reported. The triangular cantilever demonstrated an appreciable improvement in $\psi$ by 77.21% and 65.64% compared to the slender rectangular and square cantilever platforms respectively. The 2D nature of the stress generated on the cantilever platform by the surface stress loading was analyzed in detail by graphically plotting the spatial variation of the stress tensors ($\sigma_{XX}$, $\sigma_{YY}$, & $\sigma_0 = \sigma_{XX} - \sigma_{YY}$). Dimensional analysis of the triangular platform was performed to study the dependence of the electrical and the mechanical parameters on the cantilever dimensions. The profound effect of cantilever width on the magnitude of $\sigma_0$ and the resultant electrical sensitivity was analyzed considering its implications in a surface stress based sensor. A detailed dimensional analysis of the piezoresistor was performed considering the limitations of the process parameters and its influence on the electrical sensitivity of the sensor. The pervasive importance of the relative thickness of the piezoresistor to the cantilever thickness was illustrated to determine the optimal position of the neutral axis of the cantilever with respect to the midplane of the piezoresistor. The premise was demonstrated to be a tradeoff between the competing factors of the electrical

sensitivity, spring constant and measurement bandwidth. To conclude, we have presented a set of design guidelines for a triangular cantilever platform with an integrated piezoresistor for surface stress sensing applications.

## Acknowledgments

The work was supported by NPMASS, Government of India. The authors acknowledge the support of Prof Z C Alex of VIT University for arranging the facilities for simulation analysis. The authors acknowledge Mrs Meena of School of the Electronics Engineering of VIT Chennai, for her help in the simulation analysis.

## References

[1] Wasisto H S, Merzsch S, Waag A, Uhde E, Salthammer T and Peiner E 2013 Portable cantilever-based airborne nanoparticle detector *Sensors Actuator* B **187** 118–27

[2] Kim S, Yi D, Passian A and Thundat T 2010 Observation of an anomalous mass effect in microcantilever-based biosensing caused by adsorbed DNA *Appl. Phys. Lett.* **96** 153703

[3] Maute M, Raible S, Prins F E, Kern D P, Ulmer H, Weimar U and Gopel W 1999 Detection of volatile organic compounds (VOCs) with polymer-coated cantilevers detector *Sensors Actuator* B **58** 505–11

[4] Wee K W, Kang G Y, Park J, Kang J Y, Yoon D S, Park J H and Kim T S 2005 Novel electrical detection of label-free disease marker proteins using piezoresistive self-sensing microcantilever *Biosens. Bioelectron.* **20** 1932–8

[5] Li X and Lee D W 2012 Integrated microcantilevers for high-resolution sensing and probing *Meas. Sci. Technol.* **23** 022001

[6] Calleja M, Kosaka P M, Paulo A S and Tamayo J 2012 Challenges for nanomechanical sensors in biological detection *Nanoscale* **4** 4925–38

[7] Arlett J L, Myers E B and Roukes M L 2011 Comparative advantages of mechanical biosensors *Nat. Nanotechnol.* **6** 203–15

[8] Tamayo J, Ruz J J, Pini V, Kosaka P and Calleja M 2012 Quantification of the surface stress in microcantilever biosensor: revisiting Stoney's equation *Nanotechnology* **23** 475702

[9] Sader J E 2001 Surface stress induced deflections of cantilever plates with applications to the atomic force microscope: rectangular plates *J. Appl. Phys.* **89** 2911–21

[10] Sader J E 2002 Surface stress induced deflections of cantilever plates with applications to the atomic force microscope: V-shaped plates *J. Appl. Phys.* **11** 9354–61

[11] Mukhopadhyay R, Lorentzen M, Kjems J and Besenbacher F 2005 Nanomechanical sensing of DNA sequences using piezoresistive cantilevers *Langmuir* **21** 8400–8

[12] Patil S J, Duragkar N and Ramgopal Rao V 2014 An ultra sensitive piezoresistive polymer nano-composite microcantilever sensor electronic nose platform for explosive vapor detection *Sensors Actuator* B **192** 444–51

[13] Bajwa N, Maldonado C J, Thundat T and Passian A 2014 Piezoresistive measurement of swine H1N1 hemagglutinin peptide binding with microcantilever arrays *AIP Adv.* **4** 037118

[14] Pandya H J, Chen W, Goodell L A, Foran D J and Desai J P 2014 Mechanical phenotyping of breast cancer using MEMS: a method to demarcate benign and cancerous breast tissue *Lab Chip* **14** 4523–32

[15] Rasmussen P A, Thaysen J, Hansen O, Eriksen S C and Boisen A 2003 Optimised cantilever bio-sensor with piezoresistive read-out *Ultramicroscopy* **97** 371–6

[16] Zhou Y, Wang Z, Wang C, Ruan W and Liu L 2009 Design, fabrication and characterization of a two-step released silicon dioxide piezoresistive microcantilever immunosensor *J. Micromech. Microeng.* **19** 065026

[17] Boudjiet M T, Bertrand J, Mathieu F, Nicu L, Mazenq L, Leichle T, Heinrich S M, Pellet C and Dufour I 2015 Geometry optimization of uncoated silicon microcantilever-based gas density sensors *Sensors Actuators* B **208** 600–7

[18] Harley J A and Kenny T W 2000 1/*f* noise considerations for the design and process optimization of piezoresistive cantilevers *J. Microelectromech. Syst.* **9** 226–35

[19] Park S J, Doll J C and Pruitt B L 2010 Piezoresistive cantilever performance—part I: analytical model for sensitivity *J. Microelectromech. Syst.* **19** 137–48

[20] Park S J, Doll J C, Rastegar A J and Pruitt B L 2010 Piezoresistive cantilever performance—part II: optimization *J. Microelectromech. Syst.* **19** 149–60

[21] Yu X M, Thaysen J, Hansen O and Boisen A 2002 Optimization of sensitivity and noise in piezoresistive cantilevers *J. Appl. Phys.* **92** 6296–301

[22] Thaysen J, Boisen A, Hansen O and Bouwstra S 2000 Atomic force microscopy probe with piezoresistive read-out and a highly symmetrical Wheatstone bridge arrangement *Sensors Actuators* A **83** 47–53

[23] Tufte O N and Stelzer E L 1963 Piezoresistive properties of silicon diffused layers *J. Appl. Phys.* **34** 313–8

[24] Hooge F N 1972 Discussion of recent experiments on 1/*f* noise *Physica* A **60** 130–44

[25] Madou M J 2012 *Fundamentals of Microfabrication and Nanotechnology* 3rd edn (Boca Raton, FL: CRC press) 283

[26] Wang Z, Yue R, Zhang R and Liu L 2005 Design and optimization of laminated piezoresistive microcantilever sensors *Sensors Actuators* A **120** 325–36

[27] Goericke F T and King W P 2008 Modeling piezoresistive microcantilever sensor response to surface stress for biochemical sensors *IEEE Sensors J.* **8** 1404–10

[28] Kanda Y 1982 A graphical representation of the piezoresistance coefficients in silicon *IEEE Trans. Electron. Devices* **29** 64–70

[29] Thaysen J, Yalcinkaya A D, Vettiger P and Menon A 2002 Polymer based stress sensor with integrated readout *J. Phys.* D*: Appl. Phys.* **35** 2698–703

[30] Ansari M Z, Cho C and Urban G 2012 Stepped piezoresistive microcantilever designs for biosensors *J. Phys.* D*: Appl. Phys.* **45** 215401

[31] Joshi M, Gandhi P S, Lal R, Ramgopal Rao V and Mukherji S 2011 Modelling, simulation and design guidelines for piezoresistive affinity cantilevers *J. Microelectromech. Syst.* **20** 774–84

[32] Zuo G, Li X, Li P, Yang T, Cheng Y W Z and Feng S 2006 Detection of trace organophosphorus vapor with a self-assembled bilayer functionalized $SiO_2$ microcantilever piezoresistive sensor *Anal. Chim. Acta* **580** 123–7

[33] Ravi Sankar A, Lahiri S K and Das S 2009 Performance enhancement of a silicon MEMS piezoresistive single axis accelerometer with electroplated gold on a proof mass *J. Micromech. Microeng.* **19** 025008

[34] Pramanik C, Saha H and Gangopadhyay U 2006 Design optimization of a high performance silicon MEMS piezoresistive pressure sensor for biomedical applications *J. Micromech. Microeng*. **16** 2060–6
[35] Kozlovskiy S I, Nedostup V V and Boiko I I 2007 First-order piezoresistive coefficients in heavily doped *p*-type silicon crystals *Sensors Actuators* A **133** 72–81
[36] Arntz Y, Seelig J D, Lang H P, Zhang J, Hunziker P, Ramseyer J P, Meyer E, Heger M and Gerber C 2003 Label-free protein assay based on a nanomechanical cantilever array *Nanotechnology* **14** 86–90
[37] Hopcroft M A, Nix W D and Kenny T W 2010 What is the Young's modulus of silicon *J. Microelectromech. Syst.* **19** 229–38
[38] Yang S M, Yin T I and Chang C 2007 A biosensor chip by CMOS process for surface stress measurement in bioanalyte *Sensors Actuators* B **123** 707–14
[39] Richter J, Pedersen J, Brandbyge M, Thomsen E V and Hansen O 2008 Piezoresistance in *p*-type Si revisited *J. Appl. Phys.* **104** 023715
[40] Loui A, Goericke F T, Ratto T V, Lee J, Hart B R and King W P 2008 The effect of piezoresistive microcantilever geometry on the cantilever sensitivity during surface stress chemical sensing *Sensors Actuator* A **147** 516–21
[41] Tsou C, Yin H and Fang W 2001 On the out-of-plane deformation of V-shaped micromachined beams *J. Micromech. Microeng*. **11** 153–60